

XRD, TEM, EPR, IR and Nonlinear Optical Studies of Yellow Ochre

Lakshmi Reddy S^{1*}, Udayabashakar Reddy G¹, Ravindra Reddy T¹, Anita R Thomas², RamaSubba Reddy R³, Frost RL⁴ and Tamio Endo⁵

¹Department of Physics, Sri Venkateswara Degree College, Kadapa 516 003, India

²Raman Research Institute, Sadashivanagar, Bangalore 560080, India

³Department of Chemistry, Sri Venkateswara Degree College, Kadapa 516 003, India

⁴School of Chemistry, Physics and Mechanical Engineering, Queensland University of Technology, GPO Box 2434, Brisbane Queensland 4001, Australia

⁵Faculty of Engineering, Mie University, Tsu, Mie 514-8507, Japan

Abstract

Yellow ochre mineral obtained from Vempalli mandal, Cuddapah district, Andhra Pradesh of India is investigated in the present work. Its chemical analysis indicate that $\text{Fe}_2\text{O}_3=4.22$ wt% and $\text{TiO}_2=0.64$ wt%. Structural characterization is performed using X-ray diffraction (XRD). XRD results suggest that goethite (Fe_2O_3) and quartz are present. Among them goethite is the major constituent. Its unit cell is orthorhombic with $a=4.14$, $b=10.0$, $c=3.03\text{\AA}$. The ligands around the metal ion present in the structure are investigated using FTIR spectroscopy. Internal structure studied using TEM suggests that the mineral consists of needle shaped iron oxide nano particles and quartz formed as tetrahedral and octahedral layers. EPR results indicate that the unit cell of the crystal contains Fe(III), and its g values are found to be 4.19 and 2.13. FTIR properties are due to the presence of silicate and hydroxyl anions as ligands. Nonlinear optical measurements carried out using Z-scan reveal the presence of strong nonlinear optical limiting in the material, indicating potential applications in laser safety devices.

Keywords: Yellow ochre mineral; X-ray diffraction; Transmission electron microscope; Electron paramagnetic resonance; Water and silicate fundamentals; Optical limiting

Introduction

Earthy pigments varying from dull yellow to red and brown are commonly called ochres in painting. Ochres are defined [1] as clays used to make the earth colours. In pigment terminology, the word 'ochre' is predominantly used as a synonym for yellow ochre. Its colour is given by a presence of different iron oxy-hydroxides and oxides, mainly goethite and hematite. Yellow ochre is also termed as gold ochre. The brownish colour is due to the presence of manganese oxide present in the pigment [2]. Generally the soil color assessment was made according to the "Munsel soil color chart" [3]. Yellow ochre is a commercial iron oxy-hydroxide which is represented as $\text{FeO}(\text{OH})_x\text{H}_2\text{O}$ [4,5]. Since it is Fe^{3+} compound, the formula is better represented as $\text{FeO}_{1+x}(\text{OH})_{1-2x}\text{H}_2\text{O}$, $x=0$ to 0.5. Its formula is also written as $\text{Fe}_2\text{O}_6\text{Si}^{2-}$ [6]. For pigment analysis XRD, IR, Raman and EPR are the useful techniques. The sample of yellow ochre obtained from Vempalli mandal, Cuddapah district, Andhra Pradesh, India is used in the present work. In the present investigation, its chemical analysis, XRD, TEM, EPR and FTIR techniques and non linear optics are used to know the composition, crystalline phase and site symmetry of Fe^{3+} in the mineral.

Experiment

Yellow ochre sample originated from Vempalli Mandal of Cuddapah district, India is used in the present investigations. Its chemical analysis indicate that compound contains $\text{Fe}_2\text{O}_3=4.22$, $\text{TiO}_2=0.64$, $\text{CaO}=0.14$, $\text{Al}_2\text{O}_3=11.66$, $\text{SiO}_2=76.01$, $\text{MgO}=1.32$, $\text{K}_2\text{O}=2.26$ and $\text{Na}_2\text{O}=0.13$ wt%. Among them only iron and titanium are the two transition metals present in the compound. Further Fe_2O_3 and Al_2O_3 are the highest amounts in the compound. In order to identify the phase structure, XRD pattern of the mineral powder is determined by means of Philips X-ray diffractometer operated in reflection geometry at 30 mA, 40 kV with $\text{Cu}-\text{K}_\alpha$ ($\lambda=1.54060\text{\AA}$). The source is kept at 25°C. Data are collected using a continuous scan rate of 1° per 2 min which is then refined into 2 theta steps of 0.02°. TEM images are obtained using Philips CM 200 transmission electron microscope operating

at 200 kV having a resolution 0.23 nm. EPR spectra of the powdered sample are recorded at room temperature (RT) on JEOL JES-TE100 ESR spectrometer operating at X-band frequencies ($v=9.446730$ GHz), having a 100 KHz field modulation to obtain a first derivative EPR spectrum. DPPH with a g value of 2.0036 is used for g factor calculations. FTIR spectrum of the compound is recorded at RT on Perkin Elmer UV Vis-NIR spectrophotometer in powder form in the range 200-4000/cm.

Results and Analysis

XRD

XRD spectrum of yellow ochre recorded at 25°C on the Philips diffractometer is shown in Figure 1. Peaks are characterized using the Scherrner formula. It shows the presence of goethite and quartz. Among them goethite is the major constituent. The unit cell constants obtained from these peaks for goethite are $a=4.64\text{\AA}$, $b=10.0\text{\AA}$ and $c=3.03\text{\AA}$. But the JCPDS file available to this work is 3-249. This confirms that the mineral adopts orthorhombic structure. Units morphology index (MI) is developed from full width half mean (FWHM) of a peak of XRD data. The FWHM of two peaks are related with MI to its particle morphology. MI is obtained using the equation

$$MI = \frac{FWHM_h}{FWHM_h + FWHM_p}, \text{ where } FWHM_h \text{ is the highest FWHM value obtained from peaks and } FWHM_p \text{ is the value of particulars peak's FWHM for which MI is to be calculated. The MI is lying in between}$$

***Corresponding author:** Lakshmi Reddy S, Department of Physics, Sri Venkateswara Degree College, Kadapa 516003, India, Tel: +0877-2285992; Fax: +0877-2285991; E-mail: drsreddy_in@yahoo.com

Received April 27, 2015; Accepted June 29, 2015; Published June 31, 2015

Citation: Lakshmi Reddy S, Udayabashakar Reddy G, Ravindra Reddy T, Thomas AR, Rama Subba Reddy R, et al. (2015) XRD, TEM, EPR, IR and Nonlinear Optical Studies of Yellow Ochre. J Laser Opt Photonics 2: 120. doi:10.4172/2469-410X.1000120

Copyright: © 2015 Lakshmi Reddy S. This is an open-access article distributed under the terms of the Creative Commons Attribution License, which permits unrestricted use, distribution, and reproduction in any medium, provided the original author and source are credited.

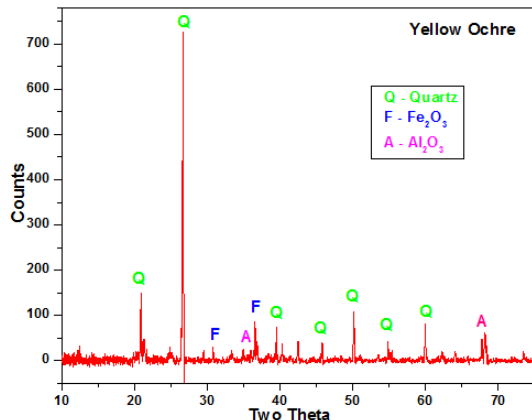


Figure 1: XRD spectrum of yellow ochre at 25°C.

0.50 and 0.88. Lorentz polarization factor is the most important of the experimental quantities that control X-ray intensity with respect to diffraction angle. In the intensity calculations Lorentz factor is combined with the polarization factor and further the variation of the Lorentz's factor with the Bragg angle (θ) is shown. The overall effect of Lorentz factor is to decrease the intensity to these in the forward or backward directions. Lorentz factor $LF = \frac{\cos\theta}{\sin^2 2\theta} = \frac{1}{4\sin^2\theta\cos\theta}$. Using the X-ray data Lorentz polarization factor is calculated using the formula $LPF = \frac{1 + \cos^2 2\theta}{\sin^2\theta\cos\theta}$ [7]. The LPF varies from 3.77 to 57.80, where LF is in between 0.87 to 7.70. The particle size of the mineral is evaluated from the line broadening of the peak (120, maximum intensity 100%) using Debye-Scherrer equation

$$D_{(120)} = \frac{0.9\lambda}{\beta_{\frac{1}{2}} \cos\theta} = 0.85\text{nm} \quad (1)$$

Here D is the particle size of the crystal, λ is the wavelength of incident X ray, θ is the corresponding Bragg angle, $\beta_{\frac{1}{2}}$ is the full width at the half maximum height (FWHM) of the peak.

The strain induced in powder due to crystal imperfection and distortion is calculated using the formula [7]

$$\eta = \frac{\beta_{hkl}}{\tan\theta} \quad (2)$$

The above two equations confirm that the peak width from crystallite size varies as $\frac{1}{\cos\theta}$ and strain varies as $\tan\theta$. Assuming that the particle size and strain contributions to line broadening are independent to each other and both have a Cauchy-like profile, the observed line breadth is simply the sum of the above two equations.

$\beta_{hkl} = \frac{k\lambda}{D \cos\theta} + \eta \tan\theta$. By rearranging we have $\beta_{hkl} \cos\theta = \frac{k\lambda}{D} + \eta \sin\theta$. A plot is drawn with $\sin\theta$ along the X-axis and $\beta_{hkl} \cos\theta$ along Y-axis for yellow ochre. From the linear fit to the data, the crystalline size is estimated from the Y-intercept as 0.62 nm. Further strain η , was calculated from the slope of the fit as 0.089. The dislocation density is calculated using the formula $\delta = \frac{1}{D^2}$ as 0.026.

Transmission electron microscope (TEM)

TEM is employed to visualize the size, shape and to confirm the

nano crystalline nature of yellow ochre. It is noticed that the yellow ochre contains several clusters and shapes. TEM images of yellow ochre are shown in Figures 2A-2D. The dark needle like rods in the Figures 2B and 2D represents Fe_2O_3 . It is observed from the image that the particles are rod in shape with almost same dimension. This property suggests that nano-crystals are preferred to instead of random orientations. These particles are very closely joined together to form agglomerates. These agglomerates are octahedral in shape, which is shown in Figure 2C. From the Figure 2A it is clear that the yellow ochre has well-defined polygonal growth forms with trimerous petals of a flower like jasmine shape and other geometrical shapes. The trimerous layers are arranged in the form of octahedral layers. These layers are appearing as "Accessible Art and Architecture in the San Francisco Area".

Further mineral in the yellow ochre size fraction is goethite. Also it can be seen that the particle size is less than 200 nm. Further from the TEM images hydroxyl clusters plus very minute clay mineral composition are noticed. TEM studies are in agreement with those values obtained from XRD analysis. Further TEM images are showing that the metal ion is in distorted octahedral structure with oxygen ligands. The selected-area electron diffraction (SAED) pattern of the yellow ochre is also shown in Figure 3. The ED pattern consists of concentric rings with spots over the rings. This feature indicates that the sample is crystalline in nature. The rings with a dotted pattern in SAED confirm the wide size distribution of Fe_2O_3 particles. Figure 3 the crystal plane d-space is measured. The measured d-spacing values are in agreement with the XRD results. Further SAED suggests that the sample possessing best crystallinity.

EPR analysis

EPR measurements are useful for obtaining information related to

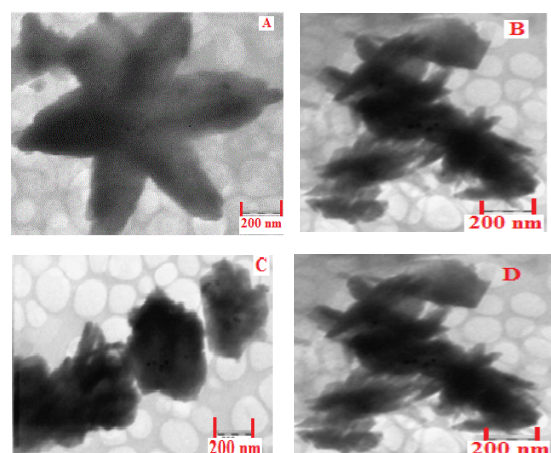


Figure 2: TEM diagrams of yellow ochre.

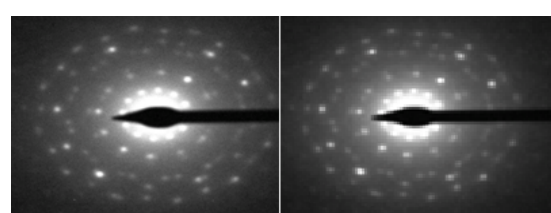


Figure 3: SAED pattern of yellow ochre.

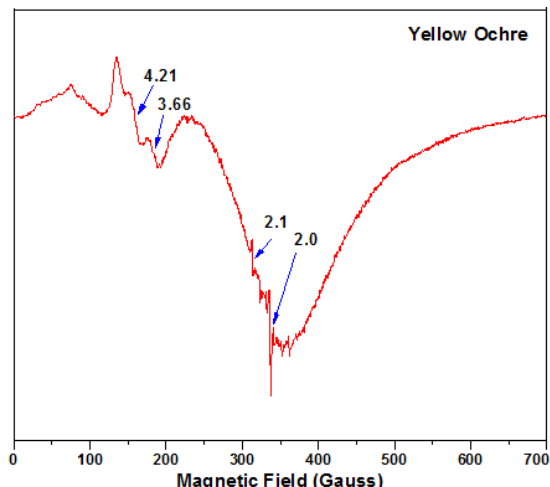


Figure 4: Room temperature EPR spectrum of yellow ochre ($\nu=9.446730$ GHz).

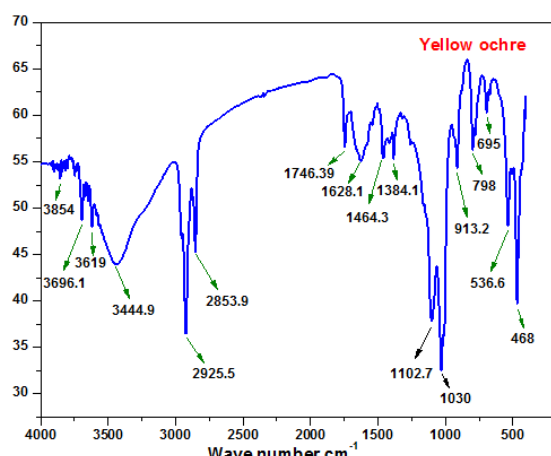


Figure 5: FTIR spectrum of yellow ochre.

the location of the transitional metal ion impurities within the lattice of the natural yellow ochre. Figure 4 shows the spectrum of the powdered yellow ochre at room temperature. It shows number of resonances. The g values of different lines are indicated in the figure. These can be explained by considering charge compensating vacancies in the lattice, when Fe^{3+} is substituted in place of Al^{3+} , it creates a low symmetry crystal field, which is further distorted because of the strong tetragonal crystal field of Fe^{3+} ion. Hence one can expect resonances from all the three Kramers doublets $|\pm 5/2\rangle$, $|\pm 3/2\rangle$ and $|\pm 1/2\rangle$. If the lowest doublet is populated, g values are obtained ranging from 0 to 9. If the middle doublet is populated gives g is 4.30 and if the third doublet is populated g values are 2/7 and 30/7. A few systems are known which show resonances from all the three Kramers doublets [8,9]. Accordingly, the EPR spectrum of the yellow ochre mineral shows with g factors ranging from 4.21, 3.66, 2.1 due to Fe^{3+} impurity. The sextet with $g=2.00$ is due Mn (II) in the mineral. Even though the chemical analysis does not show the present of manganese but the EPR is useful to detect below the chemical analysis detectable range. These results are suggesting that the majority of the yellow ochre crystals contain more than one Fe^{3+} ion in the crystal lattice.

IR Spectral analysis

The FTIR spectrum of yellow orche sample recorded in the range 4000 to 200/cm is shown in Figure 5. It shows the bands in the higher wavelength region at 1628, 1747, 2854, 2925, 3445, 3619, 3696, 3854 and lower wavelength region at 468, 537, 695, 798, 913, 1030, 1103, 1384, 1464/cm.

Water has C_{2v} symmetry. It gives three fundamental modes. They are v_1 , v_2 and v_3 . v_1 represents symmetric OH stretch, v_2 the asymmetric OH stretch and v_3 the H-O-H bend respectively [10]. In vapour phase v_1 , v_2 and v_3 occur at 3652, 1595 and 3756/cm respectively [10]. In liquid phase they are shifted to 3219, 1645 and 3445/cm, whereas in solid phase they are respectively shifted to 3200, 1640 and 3400/cm. The shifts of v_1 and v_3 towards the lower frequency side and the shift of v_2 towards the higher frequency side are indicative of hydrogen bonding [11].

A broad band at 3445/cm in the mineral is assigned to OH stretching (v_3) of structural hydroxyl groups and water present in the mineral. This indicates the possibility of the hydroxyl linkage between octahedral layers. A sharp and intense band observed at 1628/cm is due to v_2 the asymmetric OH stretch (deformation mode) of water and is a structural part of the mineral. The sharp band observed at 1463/cm may also due to OH stretch of water. The band at 2925/cm is assigned to FeOOH [12]. The band at 468/cm, which is related to the presence of quartz vibrations in yellow ochre. The maximum sharp absorption band at 1030/cm is a characteristic of Si-O-Fe and Si-O-Si stretching vibration, which play an important role in identifying ochre component. The band observed at 913/cm is assigned to OH deformation mode of Fe-OH. The band observed at 798/cm corresponds to v_1 mode. This indicates that the degeneracy is partially removed [13]. In the low wave number (below 700/cm) region, goethite has the following IR absorptions: Fe-O stretches (lattice modes of FeO_6) in the region of 600–700/cm and 450–475/cm. Accordingly the two bands observed at 695 and 468/cm are attributed to Fe-O stretching mode [14]. The band observed at 537/cm corresponds to v_2 the deformation mode of Fe-O-Si group [15]. Sharp bands observed at 2925, 2854 and 1744/cm are assigned to binder oil may present in the mineral as additive [14,16]. A sharp triply degenerate band at 1384/cm ($3 \times 468=1404$) is due to overtone of v_4 of SiO_4 .

The positions and intensities of the bands of the iron oxides vary with crystallinity, particle size, shape and the partial substitution of iron by other captions [17]. Generally, yellow iron oxide pigments contain different additives (gypsum, kaolin, quartz, and other silicate minerals) and if the additive content is high these can mask the characteristics of goethite bands. The bands observed at 468 and 537/cm are characteristic of yellow ochre [14]. These are due to additive of either quartz or kaolin present in the mineral compound.

Non-linear optics

The absorptive nonlinear optical properties of the sample was studied using Open aperture Z-scan technique at 532 nm using 5 ns laser pulses from a frequency-doubled Nd:YAG laser. The sample solution made in DMF had a linear transmission of 77% when taken in a 1 mm cuvette. The sample cuvette was translated along the axis of the focused laser beam (z axis) using a linear translation stage. Input laser pulse energy (E_n) was fixed at 60 μJ . By fixing E_n and moving the sample along the laser beam through the focal region, the incident laser fluence ($F_{in}(z)$) was gradually varied. The fluency is a maximum at the focus ($Z=0$), and reduces towards either side from the focal point (i.e., for $z>0$ and $z<0$). The transmitted energy depends on the input fluency,

and hence, on the sample position (z), for a nonlinear material.

Figure 6 shows the normalized transmission of the sample plotted against the input intensity, and the inset shows the Z-scan curve. The plots can be numerically fitted to the relevant nonlinear transmission equation, from which the nonlinear parameters can be calculated. We found that the best numerical fit to the present data can be obtained for a mechanism consisting of two-photon absorption (2PA) and weak saturable absorption (SA) [18,19]. The corresponding nonlinear absorption coefficient is given by the expression

$$\alpha(I) = \frac{\alpha_0}{1 + (I/I_s)} + \beta I \quad (3)$$

Where β is the two-photon absorption coefficient, and I_s is the saturation intensity. α_0 is the unsaturated linear absorption coefficient of the sample. The corresponding nonlinear propagation equation is given by

$$\frac{dI}{dz'} = - \left[\frac{\alpha_0}{1 + \left(\frac{I}{I_s} \right)} + \beta I \right] \quad (4)$$

Where z' is distance of propagation within the sample. By using equation (3,4) and measured data, the obtained best-fit values are $I_s = 1.7 \times 10^{12} \text{ W/m}^2$ and $\beta = 1.0 \times 10^{-10} \text{ m/W}$. From these values it is clear that Yellow ochre has strong absorptive optical nonlinearity. In the case of the present sample, excited state absorption (ESA) has a strong contribution to β compared to that of genuine two-photon absorption, and therefore, β represents the combined nonlinearity of 2PA and ESA. Thus Yellow ochre has broad application in the fabrication of optical limiters which can be used for protecting human eyes and sensitive optical detectors from harmful laser radiation because of its strong nonlinearity.

Conclusions

The following conclusions are made from the foregoing results and analysis:

- XRD investigation showed that the yellow ochre sample contained the goethite (Fe_2O_3) and quartz phases with goethite being the dominant mineral.
- TEM results are suggesting that the mineral contains goethite

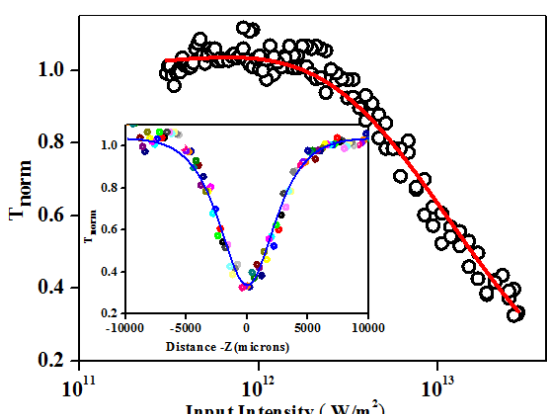


Figure 6: Nonlinear optical transmission of a DMF solution of Yellow ochre mineral, measured by the Z-scan technique. Inset shows the Z-scan curve. Circles are data points while solid curves are numerical fits to the data.

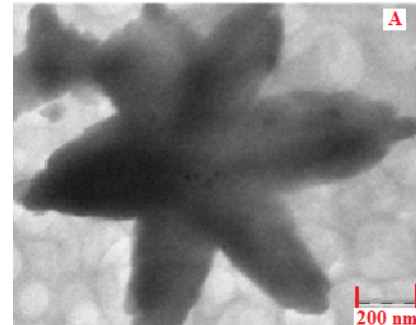


Figure 7: TEM image of yellow ochre.

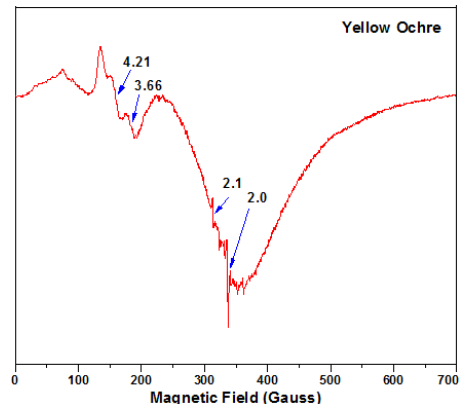


Figure 8: EPR spectrum of yellow ochre.

(iron oxide), quartz and goethite as major constituents. Further the basic unit is composed of like trimerous flower layered structure with octahedral and tetrahedral layers linked through hydroxyl groups.

- EPR spectrum is due to Fe(III) and is in distorted octahedral environment.
- IR spectrum of the compound indicating that the water and silicate are present.
- The above studies (XRD, TEM and EPR) suggesting that the coloring agent is iron oxide.
- Nonlinear optical studies carried out in the nanosecond excitation pulse regime show strong optical limiting in yellow ochre.

TOC graphic and synopsis

Yellow ochre mineral obtained from India contain $\text{Fe}_2\text{O}_3 = 4.22 \text{ wt\%}$ and $\text{TiO}_2 = 0.64 \text{ wt\%}$. Structural characterization was performed by XRD and suggesting that goethite (Fe_2O_3) as major constituent. Internal structure was studied using TEM suggests that it consists of needle shaped iron oxide nano particles and quartz formed as tetrahedral and octahedral layers. EPR results indicate that the unit cell of the crystal contains Fe(III). Nonlinear optical measurements indicating that the compound has potential applications in laser safety devices (Figures 7 and 8).

References

1. Mayer R (1991) Collins Dictionary of Art Terms and Techniques. Harper Collins, Glasgow.

2. David H, Tomas G, Janka H, Petr B (2003) Clay and iron oxide pigments in the history of painting *Applied Clay Science* 22: 223-236.
3. http://www.munsell.eu/html/munsell_color_standards.htmlhttp://www.munsell.eu/%20html/munsell_color_standards.html.
4. Ralph M (1991) *Artist's Handbook of Materials and Techniques* (5thedn.) Faber and Faber, London, Boston.
5. Richard AJ (1971) *Colour Index* The Society of Dyers and Colourists (3rdedn.) 4.
6. Webbook.nist.gov (National Institute of Standards and Technology).
7. Surayananarayana C, Grant Norton M (1998) *X-Ray diffraction: a Practical Approach*. Plenum Publishing Corporation, New York.
8. Rao PS, Subramanian S (1985) Single Crystal E.P.R. Studies of Some First-Row Transition Ions in Hexaimidazole Zinc (II) Dichloride Tetrahydrate. *Molecular Physics* 54: 415-427.
9. Castner T Jr, Newell GS, Holton WC, Slichter CP (1960) Note on the paramagnetic resonance of iron in glass. *J Chem Phys* 32: 668-673.
10. Herzberg G (1962) *Molecular Spectra and Molecular Structure*. Van Nostrand, New York 2: 167.
11. Hunt GR, Salisbury JW (1970) Visible and near-infrared spectra of minerals and rocks: I. Silicate Minerals, *Modern Geology* 1: 283-300 *Modern Geology* 1: 283.
12. Bikiaris D, Daniilia S, Sotiropoulou S, Katsimbiri O, Pavlidou E, et.al (1990) Ochre-differentiation through micro-Raman and micro-FTIR spectroscopies: application on wall paintings at Meteora and Mount Athos, Greece *Spectrochimica Acta Part A: Molecular and Biomolecular Spectroscopy* 56: 3-18.
13. Marel HWVD, Beutelspacher H (1976) *Atlas of infrared spectroscopy of clay minerals and their admixtures*. Elsevier Scientific Publishing, Amsterdam.
14. Signe V, Anu T, Ivo L (2010) ATR-FT-IR spectroscopy in the region of 550–230 cm⁻¹ for identification of inorganic pigments. *Spec Chem Acta* 75: 1061-1072.
15. Arushi G, Amitabh V, Babita K, Bivekanand M (2013) *J Pharmaceutical, Biological and Chemical Sciences (RJPBCS)* 4: 360.
16. Balakhnina IA, Brandt NN, Kimberg Ya S, Rebrikova NL, Chikishev Yu (2011) *J Appl Spectr* 78: 183.
17. Berrie BH, Feller RL, FitzHugh EW (2007) *Artists Pigments, a Handbook of their History and Characteristics*. National Gallery Art, Washington 4.
18. Ann Mary KA, Unnikrishnan NV, Reji Philip (2013) Ultrafast optical nonlinearity in nanostructured selenium allotropes. *Chemical Physical Letters* 588: 136-140.
19. Anand B, Ntim SA, Muthukumar VS, Sai SSS, Reji P, Philip R (2011) Improved optical limiting in dispersible carbon nanotubes and their metal oxide hybrids. *Carbon* 49: 4767-4773.